Soft Matter

Cite this: DOI: 00.0000/xxxxxxxxxx

Supplementary Material: Enhancing Nanoscale Viscoelasticity Characterization in Bimodal Atomic Force Microscopy

Casey Erin Adam,[a] Alba Rosa Piacenti,[a] Sarah L. Waters,[b] and Sonia Contera[a]

Received Date
Accepted Date

DOI: 00.0000/xxxxxxxxxx

[a] *Department of Physics, University of Oxford, Oxford, OX1 3PU, UK.*
[b] *Department of Applied Mathematics,Mathematical Institute, University of Oxford, OX2 6GG, UK.*

Supplementary Material

Article Title: Enhancing Nanoscale Viscoelasticity Characterization in Bimodal Atomic Force Microscopy

Authors: Casey Erin Adam, Alba Rosa Piacenti, Sarah L. Waters, and Sonia Contera

S1 Linear Viscoelasticity

A viscoelastic material has both elasticity (the elastic constant, also called Young's modulus, is written as E, with units of Pa) and viscosity (dynamic viscosity, written as η, with units of Pa s) [1–3]. If E and η are constants, not functions, the material exhibits linear viscoelasticity [1–3]. A material can have multiple components, each with a unique E, η, or both, and these components act together to dictate a material's viscoelastic response [1–3]. Material elasticity and viscosity dictate how a material responds to a stimulus, and are often used to calculate the relation between stress (force per unit area) and strain (the ratio of the difference in material dimensions during and before stimulus over material dimensions before stimulus) when a mechanical stimulus is applied to the material [1–3].

Mathematical models of viscoelasticity are often presented as equivalent circuit models, which represent the elastic components of a material's response as springs, each with a unique E, and viscous components as dampers, each with a unique η [1–3]. The standard linear solid (SLS) is the simplest model of linear viscoelasticity that fully describes both creep (changing strain under constant stress) and relaxation (changing stress under constant strain), both characteristic to viscoelastic materials [1–3]. The SLS consists of a spring and damper in series connected to a spring in parallel, as shown in figure S1 (A) [1–3].

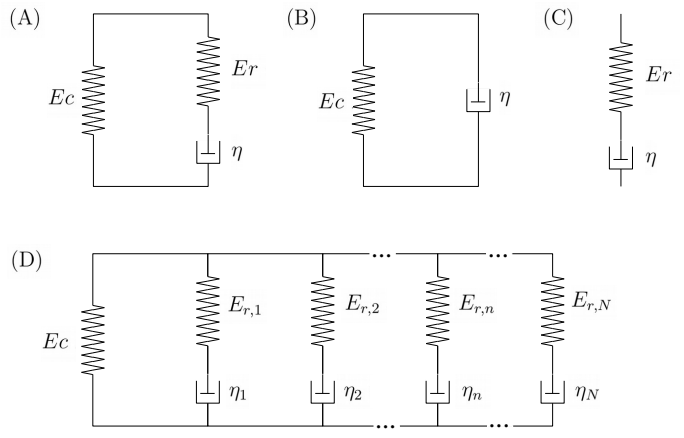

Fig. S1 Equivalent circuit models of linear viscoelasticity. Elastic components of the material are represented as springs with elastic modulus E. Viscous components are represented as dampers with dynamic viscosity η. Subscripts are used to indicate specific springs and dampers. Panel (A) shows the standard linear solid (SLS), the simplest model of linear viscoelasticity that fully describes both creep and relaxation. Panel (B) shows the Kelvin-Voigt (KV) model, which is a special case of the SLS where $E_r \to \infty$. Panel (C) shows the Maxwell (MW) model, which is another special case of the SLS where $E_c \to 0$. Panel (D) shows the generalized SLS, known as the general Maxwell model (GMM), with can be thought of as N SLSs connected in parallel.

Special cases of the SLS, where one of the elastic constants dominates the material's response, are known as the Maxwell (MW, figure S1 (C), where $E_c \to 0$) and Kelvin-Voigt (KV, figure S1 (B), where $E_r \to \infty$) models [1–4]. The SLS can also be generalized by adding additional arms of springs and dampers in parallel to the equivalent circuit, as diagrammed in figure S1 (D) [1–4]. This generalized SLS is called the general Maxwell model (GMM) or the Wiechert model [1–3]. Note that E_c of the generalized model is actually a sum of E_c from individual SLSs. Therefore, the general model can be thought of as several SLSs connected in parallel. The GMM is useful for representing complicated systems with multiple constituents and multiple time responses that dictate their mechanics [1–9]. Equivalent circuit models are used to relate stress ($\sigma(t)$, force per unit area) and strain ($\varepsilon(t)$, change in object dimensions / original dimensions), both functions of time (t) in a material undergoing mechanical stimulus. Equations S1, S2, S3, and S4 apply to the SLS, KV, MW, and GMM, respectively [10].

$$\dot{\sigma}(t) + \frac{E_r}{\eta}\sigma(t) = (E_c + E_r)\,\dot{\varepsilon}(t) + \frac{E_c E_r}{\eta}\varepsilon(t) \tag{S1}$$

$$\sigma(t) = E_c\varepsilon(t) + \eta\dot{\varepsilon}(t) \tag{S2}$$

$$\dot{\varepsilon}(t) = \frac{\dot{\sigma}(t)}{E_r} + \frac{\sigma(t)}{\eta} \tag{S3}$$

$$\left[\prod_{j=1}^{N}\left(E_j + \eta_j\partial_t\right)\right]\sigma(t) = E_c\left[\prod_{j=1}^{N}\left(E_j + \eta_j\partial_t\right)\right]\varepsilon(t) + \left[\sum_{i=1}^{N}\left(E_i\eta_i\partial_t\right)\prod_{j=1,j\neq i}^{N}\left(E_j + \eta_j\partial_t\right)\right]\varepsilon(t) \tag{S4}$$

Dynamic experiments, where an oscillatory stimulus ($\varepsilon(t) = \sin(\omega t)$) is applied to a sample, are common means of quantifying sample viscoelasticity [2,11]. Dynamic experiments do not directly measure the elastic and viscous constants of a sample, but instead quantify the storage modulus (E', Pa), loss modulus (E'', Pa) and loss tangent, $\tan\delta = E''/E'$, of a sample [2,11]. The values of E', E'', and $\tan\delta$ depend on the frequency of the applied stimulus, and are functions of the various E and η in the material [2,4,11]. The exact relation depends on the equivalent circuit model that applies to the material, and is obtained by substituting $\varepsilon(t) = \sin(\omega t)$ into the differential equation describing the stress/strain relationship of the model (equations S1, S2, S3, and S4 for the SLS, KV, MW, and GMM, respectively), solving for $\sigma(t)$, then separating the components of $\sigma(t)$ in phase (E') and out of phase (E'') with the applied stimulus [2,4,11]. Relations between E', E'', and $\tan\delta$ as functions of E and η are detailed in supplementary table S1 for the MW, KV, SLS, and GMM [2,4,11]. E and η can be calculated from experimental measurements of E', E'', and/or $\tan\delta$ if the viscoelastic model (e.g. GMM, SLS, KV, or MW) that best describes a sample is known [4].

Table S1 Relationship between viscoelastic material constants and dynamic measurement quantities. The four simplest models of linear viscoelasticity are the General Maxwell Material (GMM), standard linear solid (SLS), Kelvin-Voigt (KV), and Maxwell (MW) models. The GMM consists of N SLSs, and the MW and KV models are special cases of the SLS. Elastic (E) and viscous (η) constants within the material dictate the material's response to a dynamic stimulus at angular frequency ω, characterized by a sample's storage modulus (E'), loss modulus (E''), and loss tangent ($\tan\delta = E''/E'$). Note that the various E and η in the table below correspond to those in supplementary figure S1

Model	E' (Pa)	E'' (Pa)	$\tan\delta = E''/E'$
MW	$E' = \frac{E_r\eta^2\omega^2}{E_r^2+\eta^2\omega^2}$	$E'' = \frac{E_r^2\eta\omega}{E_r^2+\eta^2\omega^2}$	$\tan\delta = \frac{E_r}{\eta\omega}$
KV	$E' = E_c$	$E'' = \eta\omega$	$\tan\delta = \frac{\eta\omega}{E_c}$
SLS	$E' = E_c + \frac{E_r\eta^2\omega^2}{E_r^2+\eta^2\omega^2}$	$E'' = \frac{E_r^2\eta\omega}{E_r^2+\eta^2\omega^2}$	$\tan\delta = \frac{E_r^2\eta\omega}{(E_c+E_r)\eta^2\omega^2+E_r^2E_c}$
GMM	$E' = E_c + \sum_{n=1}^{N}\frac{E_n\eta_n^2\omega^2}{E_n^2+\eta_n^2\omega^2}$	$E'' = \sum_{n=1}^{N}\frac{E_n^2\eta_n\omega}{E_n^2+\eta_n^2\omega^2}$	$\tan\delta = \frac{\sum_{n=1}^{N}\left(E_n^2\eta_n\omega\prod_{j\neq n}(E_j^2+\eta_j^2\omega^2)\right)}{E_c\prod_{n=1}^{N}(E_n^2+\eta_n^2\omega^2)+\sum_{n=1}^{N}\left(E_n\eta_n^2\omega^2\prod_{j\neq n}(E_j^2+\eta_j^2\omega^2)\right)}$

S2 Macroscale Dynamic Mechanical Analysis (mDMA)

Dynamic mechanical analysis (DMA) is one of the standard tools to quantify the macroscopic viscoelastic properties of a sample [1,11–13]. DMA apparatuses exist in a variety of geometries in order to apply stimuli in different orientations relative to the surface of a sample [11–13]. The mDMA experiments in this article used axial geometry, which applies a force normal (perpendicular) to the sample's surface [11–14]. Additionally, multiple operational modes exist for mDMA apparatuses [11–14]. The mDMA experiments in this article were performed in tension mode to measure the storage (E') and loss (E'') modulus of a macroscale SBR sample [13,14]. In tension mode DMA, a sample is clamped at both ends in the apparatus, a sinusoidal force is applied to one end of the sample, and the resulting sinusoidal force F and sinusoidal axial displacement z of the sample are recorded [1,12–14]. These quantities can then be converted to E' and E'', depending on the geometry of the sample [1,12–14]. The following equations apply if the sample is rectangular, which was the case for the SBR sample used in the mDMA experiments provided for this article [13,14]. Here, H, W, and L are the undeformed thickness, width, and length of the sample, F_o is the amplitude of F, z_o is the amplitude of z, and ϕ is the phase angle between F and z [1,12–14].

$$E' = \frac{F_o L}{z_o W H}\cos\phi \tag{S5}$$

$$E'' = \frac{F_o L}{z_o W H}\sin\phi \tag{S6}$$

Additional details on SBR mDMA can be found in the works of Piacenti, 2021 and 2024 [13,14].

S3 Nanoscale Dynamic Mechanical Analysis (nDMA)

Photothermal AFM nano-dynamic mechanical analysis is a novel AFM technique to perform nanoscale dynamic mechanical analysis (nDMA) by indenting a sample with chirped frequency oscillations via photothermal actuation of the AFM cantilever [13,14]. This technique quantifies a sample's storage modulus (E'), loss modulus (E''), and loss tangent ($\tan\delta = E''/E'$) over a wide and continuous range of frequencies [13,14]. For this nDMA technique, the AFM tip indents a sample, then dwells on the sample for a time interval D, then retracts. During the dwell, the sample is allowed to fully relax [13,14]. After the sample relaxes, an oscillatory signal of varying frequency, starting at frequency f_0 and ending at frequency f_f, is applied to the sample [13]. This oscillation is called a chirp signal, and obeys the following expression [13,14]. A logarithmic chirp is used because a linear chirp causes artifacts at low frequencies [13–15].

$$f(t) = f_0 \sin\left(f_0\left(\frac{f_f}{f_0}\right)^{1/D}\right) \tag{S7}$$

For a directly actuated cantilever, the effective storage stiffness k' and loss stiffness k'' of the tip/sample interaction can be calculated for each frequency in the chirp by equating the sinusoidal force acting on the cantilever (with amplitude A_r and phase ϕ_r) when the tip is out of contact, with the force needed to deform the sample (with amplitude A and phase ϕ) [13,14,16].

$$k' = k_c\left[\frac{A_r}{A}\cos(\phi_r-\phi)-1\right] \tag{S8}$$

$$k'' = k_c\frac{A_r}{A}\sin(\phi_r-\phi) \tag{S9}$$

$$\tan\delta = \frac{k''}{k'} \tag{S10}$$

The geometric contributions to k' and k'' cancel when they are divided by one another[13,14]. Therefore, $\tan\delta$ measured by any technique is independent of the contact geometry (geometry of the tip/sample interaction)[13,14]. However, the same is not true for k' and k''[13,14]. Therefore, storage and loss moduli of a sample (E' and E'') must be obtained by applying a contact model to the expressions for k' and k''[13,14,17]. Assuming that $E_{\text{tip}} \gg E_{\text{sample}}$, the equation for E' and E'' of the sample are shown below for the Hertz contact model[13,14,17]. Equations for other contact models can be applied depending on the contact geometry between the tip and sample, as previously described[14].

$$E' = \left(\frac{1-\nu_S^2}{2a_1}\right)k' \tag{S11}$$

$$E'' = \left(\frac{1-\nu_S^2}{2a_1}\right)k'' \tag{S12}$$

Here, ν_S is the Poisson ratio of the sample, and a_1 represents the contact radius when the tip is in the sample, at the instant retraction begins[13,14]. It was assumed that $\nu_S = 0.5$ for the SBR in this article, because 0.5 is a typical ν_S for SBRs[13,14,17–20].

S3.1 Limitations of photothermal nDMA

The limitations of photothermal nDMA are similar to those of standard AFM indentation experiments[13,14]. Specifically, sample properties can be incorrectly calculated if the cantilever is softer than the sample or comparable to $|k' + ik''|$.[13,14]. Additionally, the oscillations during the dwell must be smaller than the indentation (so the tip doesn't come off the sample during the chirp), but larger than the noise floor[13,14]. For both these reasons, as well as possibly probing the properties of the underlying substrate, photothermal nDMA is difficult to perform on thin samples (only a few nanometers thick)[13,14]. An additional limitation of photothermal nDMA is that cantilever resonance causes artifacts in the data. Therefore, only off resonance frequencies can be used to excite the cantilever[13,14]. Additional analysis of factors that affect photothermal nDMA measurements and more details on SBR nDMA can be found in the works of Piacenti *et.al.*, 2021 and 2024[13,14].

S4 Bimodal AFM

Bimodal AFM is a form of tapping mode (TM) AFM. In TM, a cantilever is driven by an AC voltage so that the tip intermittently taps the surface of the sample at a specific frequency[21–24]. This frequency is usually the resonance frequency of the cantilever's first eigenmode[22–24]. An eigenmode is a natural resonance mode of the cantilever, and occurs at a specific frequency[22–24]. This eigenfrequency is called a resonance frequency when the applied frequency matches the eigenfrequency[22–24].

In standard TM, the amplitude (A) of the cantilever's oscillation is kept constant[22–25]. This feedback on the amplitude is called amplitude modulation (AM)[22–25]. Other forms of TM maintain a constant phase (ϕ) for phase modulation (PM), or a constant frequency (f) for frequency modulation (FM)[26].

While TM is typically used to obtain high resolution images of nanoscale or atomic-scale features of a sample's surface[25], additional information beyond sample topography is contained in ϕ and f[22–24]. During a TM experiment, tip/sample interaction forces shift ϕ and f by some $\Delta\phi = \phi - \phi_c$ and $\Delta f = f - f_c$, where ϕ_c and f_c are the reference phase and amplitude of the cantilever's oscillation far from the sample[22–24]. In standard TM, $\phi_c = 90^o$ and f_c is the resonance frequency of the cantilever[22–24]. If the tip and sample have a repulsive interaction, $\Delta\phi < 0$ and $\Delta f > 0$[22–24,27]. The reverse is true for an attractive interaction, $\Delta\phi > 0$ and $\Delta f < 0$. Therefore, the mechanics of a sample can be quantified in a TM experiment by closely tracking $\Delta\phi$ or Δf[22–24,28].

Bimodal TM allows close tracking of $\Delta\phi$ and Δf as well as sample topography[25,26,29]. In bimodal TM, the tip is driven at two eigenmodes, usually the lowest two, instead of one, and two feedback loops are employed on the cantilever's vibration[25,26,29]. Like standard TM, bimodal imaging can provide high-resolution maps of a sample's surface[25,26,29]. Unlike standard TM, the additional observables of the second eigenmode (A_2, ϕ_2, and f_2 in addition to A_1, ϕ_1, and f_1) allow more of the sample's mechanical properties to be quantified[25,26,29].

In bimodal AFM, the first mode of the cantilever (the lower frequency eigenmode) is typically subject to AM, as in standard TM[25,26,29]. The second mode can be subject to AM (for AM-AM AFM), PM (for AM-PM AFM), or FM (for AM-FM AFM)[25,26]. The equations relating bimodal observables in any of these configurations to the mechanical properties of a sample are interchangeable[26]. AM-FM AFM is slightly more accurate than AM-AM or AM-PM because AM-FM makes the second mode less likely to experience a drop in signal-to-noise-ratio[26]. Therefore, AM-FM AFM is typically used for quantifying sample viscoelasticity[26].

S4.1 AM-FM AFM

In AM-FM AFM, the AM feedback operating on the lower eigenmode, quantifies the height of features on the sample's surface[25,29]. Additionally, the ratio of power dissipated over power stored by the first mode's vibration provides the loss tangent ($\tan\delta$) of the sample[30,31].

$$\tan\delta = \frac{\sin(\phi_1) - \frac{A_1}{A_{r,1}}}{\cos(\phi_1)} \tag{S13}$$

Here, ϕ_1 is the phase of mode one, A_1 is the amplitude of mode one while interacting with the sample, and $A_{r,1}$ is the reference amplitude of mode one far from the sample (also called the free amplitude). Equation S13 is negative if $\phi_1 > 90^o$. Therefore, the tip and sample must exhibit a repulsive interaction for equation S13 to apply[27,30,31]. A repulsive interaction is typically achieved by pushing hard on the sample (the amplitude setpoint is less than 75% of the free amplitude) and by using a sharp tip[26,27,29].

The higher eigenmode is frequency-modulated (FM), and closely tracks the frequency shift of the cantilever due to tip/sample interactions, Δf_2[25,26,29,32]. Specifically, $\Delta f_2 = f_2 - f_{c,2}$, where f_2 is the frequency of mode two on the sample, and

$f_{c,2}$ is the resonance frequency of the second eigenmode[29]. An additional feedback loop for the second mode, called a dissipation feedback loop, helps prevent the amplitude of the second mode from dropping below the detection limit if large frequency shifts occur[25,29,32]. The dissipation feedback loop alters the drive amplitude of the second mode in order to ensure that the mode has a high enough amplitude (above the noise floor), and is not used in AM-FM AFM calculations[29]. The FM loop, Δf_2, is used to solve for E' of the sample by relating Δf_2 to Δk_2 to the contact modulus ($E'_{t/s}$, a convolution of tip and sample E') by applying fractional calculus[32] or bimodal interaction theory and the Hertz contact model[26]. The latter derivation is summarized here.

As the tip contacts a sample during AM-FM AFM, tip/sample interactions shift the stiffness of the cantilever at each eigenmode by some Δk[26]. Expressions for Δk of each eigenmode are obtained by modeling the cantilever's motion at each eigenmode as a simple harmonic oscillator (SHO)[26]. The Δk of each mode are then used to calculate the contact modulus, $E'_{t/s}$, by applying the Hertz contact model for spherical tip geometry, as well as bimodal interaction theory (integrating Δk over the profile of the tip for each eigenmode)[26,32].

$$E'_{t/s} = \frac{4\sqrt{2A_1}k_{c,2}^2 Q_{c,1}\left(\Delta f_2\right)^2}{\sqrt{R}k_{c,1}A_{r,1}f_{c,2}^2\cos\phi_1} \tag{S14}$$

Here, $E'_{t/s}$ is the contact modulus (which converts to sample E'), A and ϕ are the amplitude and phase of the cantilever's oscillation, A_r is the free amplitude of the cantilever (amplitude far from the sample), k_c and Q_c are the cantilever stiffness and quality factor when not interacting with a sample, f_c is the resonance frequency of the eigenmode (when not interacting with a sample), Δf_2 is the frequency shift of the second mode when the tip interacts with the sample (subject to frequency modulation), R is the radius of the tip, and the subscript 1 or 2 indicates that a quantity respectively belongs to the first or second eigenmode. While parameters from both the first and second mode are used in equation S14, the feedback is more sensitive to changes in the second mode, and hence the second mode contributes most to the measured E'[26]. In order to apply bimodal interaction theory to obtain equation S14, it is assumed that $A_2 \ll A_1$[25,26]. Therefore, it is recommended that $A_2 \leq 10\%$ of A_1 during AM-FM AFM experiments[29]. Alternative formulations for the calculation of E'_2 that rely on different contact models or different tip geometries are derived via fractional calculus by Herruzo *et. al.*, 2012[32].

Once $E'_{t/s}$ is known, E' of the sample can be calculated via the following relation[3]. Here, the subscript I represents the indenter (the tip), subscript S represents the sample, and ν represents the Poisson ratio of the indenter or sample[3].

$$\frac{1}{E'_{t/s}} = \frac{1-\nu_I}{E'_I} + \frac{1-\nu_S}{E'_S} \tag{S15}$$

For the AC240TSA and AC160TSA cantilevers used in this study, $\nu_I = 0.17$, per the Oxford Instruments Asylum Research software. If the cantilever is more-rigid than the sample, $E'_I >> E'_S$, equation S15 simplifies to equation S16[3].

$$E'_S \approx E'_{t/s}\left(1-\nu_S\right) \tag{S16}$$

It was assumed that $\nu_S = 0.5$ for the SBR in this article, because 0.5 is a typical ν_S for SBRs[13,14,17–20].

S4.2 Limitations of Bimodal AFM

AM-FM AFM, as well as other bimodal AFM techniques, must be performed with a repulsive tip/sample interaction and with $A_2 \leq 10\%$ of A_1[31]. In addition to these conditions, there are several factors that can affect AM-FM AFM measurements. First, indentations in AM-FM AFM are typically only a few nanometers[25]. While these small indentations allow high-resolution maps of the sample, are less-likely to damage the sample, and allow AM-FM AFM to be performed on thin samples, they also increase the likelihood of incorrectly estimating E' and $\tan\delta$ due to moisture layers (only applicable to dry samples) or variations in sample topography[25,31]. Second, the E' calculation for AM-FM AFM relies on the assumption that the Hertz contact model applies to the tip/sample interaction[25,26]. This assumption is erroneous if a sample adheres to the tip. Therefore AM-FM AFM can give incorrect quantification of E' on adhesive samples[25,26]. Third, certain types of dissipation (like adhesion, squeeze film dampening, or sample plasticity) can result in a calculated $\tan\delta$ higher than its actual value[31]. Fourth, due to the limits of the AFM, it is difficult for AM-FM AFM to accurately measure $\tan\delta$ less than 0.1 or higher than 10[31]. In order to minimize the possibility that the measured E' or $\tan\delta$ are incorrect due to any of these issues, AM-FM AFM can be performed in conjunction with other techniques like nDMA, or with an mDMA reference.

S5 Propagating tip radius uncertainty in Bimodal AFM calculation of sample E'_2

AM-FM AFM quantifies E'_2 of a sample via equation S14.

$$E'_{\text{eff}} = \sqrt{\frac{2}{RA_1}}\frac{\Delta k_2^2}{\Delta k_1} = \frac{Q}{\sqrt{R}}$$

Knowledge of the tip radius R is required in order to apply equation S14. In the case that R is calibrated, the user manually enters R into the software after taking AM-FM AFM measurements on a calibration sample. Therefore, R is treated as a constant. In this case, the error (S) of E' only depends on the error in Q as follows.

$$\begin{aligned}
\sqrt{R}\left(S_{E',\text{calibrated}}\right) &= S_Q \\
\sqrt{R}\left(\frac{S_{E'}}{|\overline{E'}|}\right)_{\text{calibrated}} &= \left(\frac{S_Q}{|\overline{E'}|}\right) \\
&= S_Q\left|\frac{\sqrt{R}}{Q}\right| \\
\left(\frac{S_{E'}}{|\overline{E'}|}\right)^2_{\text{calibrated}} &= \left(\frac{S_Q}{|\overline{Q}|}\right)^2
\end{aligned} \tag{S17}$$

If the radius R is not calibrated, the mean tip radius, $\overline{R}$, and the standard deviation in the radius, S_R, can be obtained from the tip specifications provided by the manufacturer. For this article, the range of radii listed by the manufacturer was used to provide a worst case estimate of S_R. The error in R can then be propagated to the error in E' as follows.

$$\left(\frac{S_{E'}}{|\overline{E'}|}\right)_{\text{uncalibrated}} = \sqrt{\left(\frac{S_Q}{|\overline{Q}|}\right)^2 + \left(\frac{1}{2}\frac{S_R}{|\overline{R}|}\right)^2}$$

$$\left(\frac{S_{E'}}{|\overline{E'}|}\right)^2_{\text{uncalibrated}} = \left(\frac{S_Q}{|\overline{Q}|}\right)^2 + \left(\frac{1}{2}\frac{S_R}{|\overline{R}|}\right)^2 \tag{S18}$$

The difference in the error of E' with uncalibrated and calibrated R is the difference between equation S18 and S17.

$$\left(\frac{S_{E'}}{|\overline{E'}|}\right)^2_{\text{uncalibrated}} - \left(\frac{S_{E'}}{|\overline{E'}|}\right)^2_{\text{calibrated}} = \left(\frac{1}{2}\frac{S_R}{|\overline{R}|}\right)^2$$

$$\left(\frac{S_{E'}}{|\overline{E'}|}\right)_{\text{uncalibrated}} = \sqrt{\left(\frac{1}{2}\frac{S_R}{|\overline{R}|}\right)^2 + \left(\frac{S_{E'}}{|\overline{E'}|}\right)^2_{\text{calibrated}}} \tag{S19}$$

If R is not calibrated, the standard deviation in the measured E' is larger than what it appears from the raw data. The standard deviation of E' from the raw data can be used to calculate the *calibrated* term of equation S19. This observation, along with manufacturer values for S_R and $|\overline{R}|$, allow calculation of the error in E' when R is not calibrated via equation S19. Equation S19 corresponds to equation 23 in section 3 of the main article.

S6 Modification of the model test for a GMM

For GMM materials, it is not possible to directly relate the value of the slope and y-intercept of the model test line (where $y = \tan\delta_1^{-1}$, $x = (E_2'\tan\delta_1)^{-1}$, and subscripts indicate the eigenmode at which the quantity was measured, equation 12) to GMM material properties because there are too few bimodal AFM observables and too many unknowns, even if only a subgroup of GMM arms is excited. The unknowns include: E_1', $\tan\delta_2$, E_1'', E_2'', E_c, the number of arms N (in the material as a whole or even a subset consisting of more than one arm), and the N different E_n (corresponding to $E_{r,n}$ in figure S1 (D), written as E_n here for simplicity) and η_n. However, it is possible to place an upper bound on E_c from the model test line as follows. First, it is necessary to acknowledge the following three facts about the GMM.

Fact one, the GMM equation for E_2' is as follows (table S1).

$$E_2' = E_c + \sum_{n=1}^{N} \frac{E_n\eta_n^2\omega_2^2}{E_n^2 + \eta_n^2\omega_2^2} \tag{S20}$$

For ease of writing, the variable χ can be introduced as follows.

$$\chi = \sum_{n=1}^{N} \frac{E_n\eta_n^2\omega^2}{E_n^2 + \eta_n^2\omega^2} \tag{S21}$$

Therefore, equation S20 can be written as follows for the measured E_2', with the subscript 2 indicating the second eigenmode at angular frequency ω_2.

$$E_2' = E_c + \chi_2 \tag{S22}$$

Fact two, for low frequencies, $\omega \to 0$, and $E' \to E_c$. For high frequencies, $\omega \to \infty$,

$$\chi \to \sum_{n=1}^{N} E_n \tag{S23}$$

and $E' \to E_c + \sum_{n=1}^{N} E_n$. Therefore, there are two plateaus in E', one at low frequencies and one at high frequencies. The value of E' never decreases with increasing frequency. Therefore, depending on the value of χ at a given frequency, the following is true for any E_1' and E_2' measured at $\omega_1 < \omega_2$.

$$\chi_1 \le \chi_2 \leftrightarrow E_1' \le E_2' \tag{S24}$$

Fact three, the GMM equation for $\tan\delta_1$ (table S1) is as follows.

$$\tan\delta = \frac{E''}{E'} = \frac{E''}{E_c + \chi} \tag{S25}$$

The first step in relating m_{GM} and b_{GM} to GMM material properties is to relate $\tan\delta_2$ and $\tan\delta_1$ using equation S25, then algebraically rearranging this relation to solve for E_c as follows.

$$\frac{\tan\delta_2}{\tan\delta_1} = \frac{E_2''E_1'}{E_1''E_2'} = \frac{E_2''E_c + E_2''\chi_1}{E_1''E_c + E_1''\chi_2} \tag{S26}$$

Rearranging provides an expression for E_c.

$$E_c = \frac{\chi_1 - \frac{\tan\delta_2 E_1''}{\tan\delta_1 E_2''}\chi_2}{\frac{\tan\delta_2 E_1''}{\tan\delta_1 E_2''} - 1} \tag{S27}$$

Next equation S25 can be employed to eliminate $\tan\delta/E''$ from equation S27 in favor of E'.

$$E_c\left(\frac{E_1'}{E_2'} - 1\right) = \chi_1 - \frac{E_1'}{E_2'}\chi_2 \tag{S28}$$

Note that the left side of equation S28 is zero if $E_c = 0$ or $E_1' = E_2'$. By equation S24, $E_1' < E_2'$. Therefore, $E_1'/E_2' - 1 < 0$. Hence, from equation S28, the following inequality results.

$$\chi_1 < \frac{E_1'}{E_2'}\chi_2 \tag{S29}$$

Adding E_c to both sides of equation S29 results in the following.

$$\chi_1 + E_c < \frac{E_1'}{E_2'}\chi_2 + E_c \tag{S30}$$

Recalling that $\tan\delta = E''/E'$ and substituting into equation S30 results in the following inequality.

$$E_1' < \frac{E_1'}{E_2'}\chi_2 + E_c \tag{S31}$$

Hence, the following is true.

$$\frac{1}{\tan\delta_1} < \frac{\chi_2}{\tan\delta_1 E_2'} + \frac{E_c}{E_1''} \tag{S32}$$

The inequality can be rearranged as follows. Here, m_{GM} and b_{GM} are the slope and y-intercept of the model test line fit to data from a GMM material.

$$\frac{m_{\mathrm{GM}}}{\tan\delta_1 E_2'} + b_{\mathrm{GM}} = \frac{1}{\tan\delta_1} < \frac{\chi_2}{\tan\delta_1 E_2'} + \frac{E_c}{E_1''} \tag{S33}$$

Rearranging further results in the following relation.

$$\frac{(m_{\mathrm{GM}} - \chi_2)}{\tan\delta_1 E_2'} + b_{\mathrm{GM}} - \frac{E_c}{E_1''} < 0 \tag{S34}$$

Equation S34 can be used to obtain a bound for E_c by substituting $E_2' - E_c$ for χ_2 and algebraically rearranging as follows.

$$\frac{m_{\mathrm{GM}}}{E_2'} - \frac{\chi_2}{E_2'} + \tan\delta_1 b_{\mathrm{GM}} - \frac{E_c}{E_1'} < 0$$

$$\frac{m_{\mathrm{GM}}}{E_2'} - 1 + \frac{E_c}{E_2'} + \tan\delta_1 b_{\mathrm{GM}} - \frac{E_c}{E_1'} < 0$$

$$-\frac{m_{\mathrm{GM}}}{E_2'} + 1 - \tan\delta_1 b_{\mathrm{GM}} + \frac{E_c}{E_1'} > \frac{E_c}{E_2'} \tag{S35}$$

To place a bound on E_c, it is necessary to eliminate the remaining unknown, E_1', from the relation. This task can be accomplished by defining $\alpha = E_c/E_1'$. From GMM fact two, $0 < \alpha \leq 1$. Equation S35 then becomes the following.

$$E_c < (1+\alpha)E_2' - m_{\mathrm{GM}} - E_2'\tan\delta_1 b_{\mathrm{GM}} \tag{S36}$$

Next, the limits of α can be substituted into equation S36, and E_c can be estimated by assuming that the value of E_c is equal to the bound. The most restrictive bound on E_c occurs when $\alpha = 0$, resulting in the following.

$$E_c < E_2' - m_{\mathrm{GM}} - E_2'\tan\delta_1 b_{\mathrm{GM}}$$

$$E_c \sim E_2'(1 - \tan\delta_1 b_{\mathrm{GM}}) - m_{\mathrm{GM}} \tag{S37}$$

For kHz frequencies such as those in bimodal AFM, E_c can often be several orders of magnitude smaller than E' because polymers in the material have less time to rearrange in response to kHz frequencies than lower frequencies[1,2]. Therefore, the bound of $\alpha \sim 0$, and equation S37 (equation 17 in the main text), are likely to apply.

The least restrictive bound on E_c occurs when $\alpha = 1$, resulting in the following (equation 18 in the main text).

$$E_c < 2E_2' - m_{\mathrm{GM}} - E_2'\tan\delta_1 b_{\mathrm{GM}}$$

$$E_c \sim E_2'(2 - \tan\delta_1 b_{\mathrm{GM}}) - m_{\mathrm{GM}} \tag{S38}$$

Note that the condition in equation S38 is satisfied when equation S37 is satisfied.

Since the value of E_c is estimated by assuming that E_c is close to E_c's upper bound, the most restrictive estimate of the bound should be used when possible. For example, if $\alpha = 0.1$, and equation S38 is used, then E_c will be set to a value $(E_2'(2 - \tan\delta_1 b_{\mathrm{GM}}) - m_{\mathrm{GM}})$ higher than possible $(E_2'(1.1 - \tan\delta_1 b_{\mathrm{GM}}) - m_{\mathrm{GM}})$, and will therefore be incorrect. However, if α is closer to 1, the most restrictive bound could yield an incorrectly low, and possibly nonphysical, estimate of E_c. In this case, equation S38 should be used instead. If mDMA or nDMA control measurements are available for a sample, the value of α, and hence which equation to use can be estimated by comparing E' at low frequencies to E' at the measurement frequencies. If such controls are not available, equation S37 should be used unless nonphysical, for example negative, values of E_c result from applying equation S37.

After approximating E_c from equation S37 or S38, rough values for the other material constants of the GMM can be obtained from the upper bound of E_c and the bimodal AFM observables as described in section 2.2 of the main text. However, such calculation should only be employed after determining whether the assumptions leading to equation S37 are valid for each cantilever/sample pair, specifically whether the actual value of E_c is indeed close to the bound of E_c and whether equation S38 or S37 should be used.

Since it is necessary to assume that E_c is approximately its upper bound, it is therefore possible to inaccurately estimate the value of a GMM's E_c using this method. However, as discussed in the main article (table 1), this assumption is still more accurate than applying the same manipulations for the SLS to the GMM (section 2.1 of the main text), since $m_{\mathrm{GM}} \neq E_c$, per relation S35. Additionally, the accuracy of assuming that the actual value of E_c is close to the upper bound of E_c may depend on the cantilever/sample paring, as shown by figure 5 and supplementary figure S2 where the value of E_c is less accurate in the reconstruction from the AC160TSA compared to that of the AC240TSA. Since f_1 and f_2 are higher for the AC160TSA, these results suggest that the upper bound of E_c may be less accurate when higher measurement frequencies are used in the calculation. It is reasonable to hypothesize that, the higher the measurement frequencies, the sample's behavior at low frequencies is less certain, and therefore, the bound in E_c is also less certain. As discussed in the main text, if it is important to be more certain of the value of E_c, it is better to use nDMA to directly measure the sample's viscoelastic behavior at low frequencies. However, the analysis described here can still be used to approximate E_c of a GMM as long as the assumption that the true value of E_c is close to the upper bound of E_c, and the limitations of this assumption, are acknowledged. This assumption will not be valid for all materials. Therefore, for such a relation to be used to calculate GMM material constants, it is best to have control data, such as the DMA data in this article, to ensure the assumption holds. If the assumption fails, analysis should stop after the model test line (main text section 2.1) in order to avoid incorrectly calculating material constants.

S7 Alternative Method to that Described in Section 2.2 for Estimating Sample Properties

Directly calculating material constants as described in section 2.2 requires solving a cubic polynomial for τ_r (equation 21). This section provides an alternate way of calculating material constants if there are no real or positive roots for the cubic polynomial. While such a situation is not physical, such roots can arise if the polynomial is flat in the vicinity of the roots, which increases the influence of machine error on numerical outputs of the root solv-

ing function. For such cases, the alternate method plots bimodal AFM data in a second line (after the model test line, equation 12), and hence has greater uncertainty than the procedure described in section 2.2 due to the fact that fit parameters of the second line will also carry uncertainty.

Once E_c is known, plotting bimodal AFM data in a second line can be used to solve for the remaining material constants for samples that do not obey the KV model. The slope and y-intercept of the model test line (equation 12) can be used to calculate E_c for the SLS and the upper bound of E_c for a GMM. $E_c = 0$ for MW materials. The remaining material constants (E_r, η, $\tau_r = \eta/E_r$, and $\tau_c = \eta/E_c$) can be determined from E_2', $\tan\delta_1$, and E_c via the expressions for E' and $\tan\delta$ of the SLS (equation 5 and 7, respectively).

First, equation 7) can be rearranged to solve for $E_c + E_r$ as follows.

$$E_c + E_r = \frac{\eta\omega - E_c\tan\delta}{\tau_r^2\omega^2} \tag{S39}$$

Similarly, equation 5 can also be rearranged to solve for $E_c + E_r$.

$$E_c + E_r = E' + \frac{E' - E_c}{\tau_r^2\omega^2} \tag{S40}$$

Equating equation S39 at the first cantilever eigenmode in bimodal AFM with equation S40 at the second eigenmode provides the following relation.

$$\frac{\eta\omega_1 - E_c\tan\delta_1}{\tau_r^2\omega_1^2} = E_2' + \frac{E_2' - E_c}{\tau_r^2\omega_2^2} \tag{S41}$$

Recalling that E_c is known from equation 12, equation S41 can be algebraically rearranged so that the left hand side consists only of known quantities as follows.

$$\frac{\tan\delta_1}{\omega_2^2}\left[E_c + \frac{\omega_1^2}{\omega_2^2}\left(E_2' - E_c\right)\right] = -E_2'\tan\delta_1\omega_1^2\tau_r^2 + \eta\omega_1 \tag{S42}$$

Since E_c is known, the left hand side of equation S42 is known. A plot of $\tan\delta_1\left[E_c + \omega_1^2\left(E_2' - E_c\right)/\omega_2^2\right]/\omega_2^2$ against $-E_2'\tan\delta_1\omega_1^2$ should be linear, with a slope $m_2 = \tau_r^2$ and a y-intercept $b_2 = \eta\omega_1$. Therefore, $\tau_r = \sqrt{m_2}$, and $\eta = b_2/\omega_1$. E_r can then be calculated as $E_r = \eta/\tau_r$, and $\tau_c = \eta/E_c$. Note that parameter calculation from equation S42 should only be performed if the sample is a MW, SLS or GMM material, and if the calculations described in section 2.2 are for some reason undesirable. If the material is a KV material, equations 1 through 4 should be used to calculate the sample's material constants instead.

S8 Gaussian Fitting to AM-FM AFM Data

As shown in figure 1, distributions of the measured E_2' and $\tan\delta_1$ were sometimes multimodal. Therefore, calculating the mean and standard deviation via the standard formulas may not represent the data well (also shown in figure 1). To overcome this issue, distributions from individual AM-FM AFM images, as well as the distribution of data from all images, were fit with single term and two term Gaussians, $g(x)$, to calculate the mean and standard deviation.

The equation for the single term Gaussian, and the calculations to obtain the mean, $|\overline{X}|$, and standard deviation, S, from this fit are shown in equations S43 through S45.

$$g_1(x) = a_1 e^{-\left(\frac{x-b_1}{c_1}\right)^2} \tag{S43}$$

$$|\overline{X}| = b_1 \tag{S44}$$

$$S = \sqrt{\frac{c_1^2}{2}} \tag{S45}$$

Similarly, the equation for the two term Gaussian, and the calculations to obtain $|\overline{X}|$ and S of each peak from this fit are shown in equations S46 through S48

$$g_2(x) = a_1 e^{-\left(\frac{x-b_1}{c_1}\right)^2} + a_2 e^{-\left(\frac{x-b_2}{c_2}\right)^2} \tag{S46}$$

$$|\overline{X}|_1 = b_1 \text{ and } |\overline{X}|_2 = b_2 \tag{S47}$$

$$S_1 = \sqrt{\frac{c_1^2}{2}} \text{ and } S_2 = \sqrt{\frac{c_2^2}{2}} \tag{S48}$$

To determine whether $g_1(x)$ or $g_2(x)$ best describes the data, if less than 35% of each Gaussian in the two term fit overlapped, $g_2(x)$ was used to represent the distribution, and equations S47 and S48 to calculate $|\overline{X}|_1$, S_1, $|\overline{X}|_2$, and S_2. Otherwise, if more than 35% of each Gaussian overlapped $g_1(x)$ was used for the data.

If $g_1(x)$ was used, equations S44 and S45 were used to calculate $|\overline{X}|$ and S. If $g_2(x)$ was used, $|\overline{X}|$ and S were calculated from either $|\overline{X}|_1$ and S_1 or $|\overline{X}|_2$ and S_2 by selecting the Gaussian (corresponding to $|\overline{X}|_1$ and S_1, or to $|\overline{X}|_2$ and S_2) with $|\overline{X}|$ closest to the value that had the highest count in the distribution. Therefore, $|\overline{X}|$ and S calculated from this procedure represent the most prominent peak in the distribution, which corresponds to the most prevalent component of the distribution, and therefore of the sample.

S9 Cross-Validating Analysis Procedure Outputs

Analysis procedure outputs can be compared against a variety of other measurements in order to ensure that parameter estimates are reasonable, and that the assumptions used to obtain these estimates apply (for example, assuming that E_c of a GMM is close to the bound of E_c, main text section 2.1.1 and supplementary section S6). Measurements that can be used to cross-validate analysis procedure outputs include: mDMA, nDMA, nanoindentation, relaxation experiments, creep experiments, and literature measurements of similar samples. The pros and cons of each cross-validation measurement are elaborated in the following sections.

S9.1 Cross-Validation using mDMA

If mDMA measurements are used as a control for cross-validation, it is important to consider the fact that, for many polymeric materials, nanoscale properties such as E' and E'' can be several orders of magnitude higher than macroscale properties due to the natural scaling behavior of the polymers within the material[33]. While the SBR sample in this article did not exhibit such scaling[13,14], this will not be the case for all samples, especially biolog-

ical samples[33]. Furthermore, since nanoscale measurements only probe a small portion of a sample, nanoscale measurements can be more susceptible to local variations in sample structure than macroscale measurements[13]. Such variations between nanoscale and macroscale measurements could also contribute to scaling behavior. Additionally, as was the case in the main article, bimodal AFM measurements of E_2' might not match mDMA if the Hertz model, employed in bimodal AFM's calculation of E_2'[26,32], does not apply. However, mDMA can still be used to cross-validate analysis procedure outputs as long as scaling and contact model are considered.

To cross-validate bimodal AFM outputs with mDMA, it is necessary to first determine if scaling or contact model effects are present by checking whether bimodal $\tan\delta_1$ agrees with mDMA at f_1 ($\tan\delta(f_1)$) and whether E_2' agrees with mDMA E' at f_2 ($E'(f_2)$). If $\tan\delta_1 \neq \tan\delta(f_1)$, it is possible that bimodal imaging parameters were not properly selected (see main text figure 2) a different cantilever may be required to accurately measure the sample, or effects such as adhesion, squeeze film damping, or sample plasticity are present[31] and bimodal AFM measurements should be repeated. Otherwise, $\tan\delta_1 = \tan\delta(f_1)$ should hold true. If $E_2' = E'(f_2)$, then no scaling behavior is present and the Hertz model adequately describes the tip/sample interaction during bimodal measurements. If $\tan\delta_1$ agrees with mDMA, but $E_2' \neq E'(f_2)$, then contact model or scaling effects are present. If changing the contact model resolves the discrepancy between bimodal E_2' and mDMA (as was the case for the SBR in this article[13,14]), then the Hertz model does not accurately describe the tip/sample contact. If changing the contact model does not resolve the discrepancy between E_2' and $E'(f_2)$, then scaling behavior is present. Regardless, $E_2' + \Delta E$ should agree with $E'(f_2)$, where ΔE represents discrepancies due to scaling or contact model effects. Without such effects, $\Delta E = 0$.

If the sample obeys the GMM or any of the GMM's special cases, the analysis procedure in this article can be used to estimate model parameters and reconstruct $E'(f)$, $E''(f)$, and $\tan\delta(f)$ (main text section 2.3). If the sample does not obey the GMM or any of the GMM's special cases, the model is unknown, and the therefore sample parameter estimation should not be performed (see main text figure 6). However, for samples obeying the GMM, SLS, KV, or MW models, the shape of reconstruction curves and the value of E_c can be cross-validated against mDMA.

Curve shapes should be similar between reconstructions and mDMA. If the sample obeys the SLS, KV, or MW model, reconstruction $\tan\delta(f)$ should match mDMA $\tan\delta(f)$. Additionally, reconstruction $E'(f)$ and $E''(f)$ should match mDMA $E'(f) + \Delta E$ and $E''(f) + \Delta E$, respectively. If the sample is a GMM, reconstruction shapes are more likely to match mDMA closer to bimodal measurement frequencies, but start to deviate from mDMA at frequencies far from f_1 and f_2 because the analysis procedure reconstructs GMM samples with SLS equations (see main text section 2.3, figure 5 and supplementary figure S2).

Estimated E_c can also be compared against mDMA. For the GMM and special cases of the GMM, $E' = E_c$ when $f \sim 0$ (formulas in supplementary table S1). Therefore, analysis procedure $E_c + \Delta E$ should match mDMA E' at low frequencies. For GMM samples, the procedure calculates GMM E_c by assuming that the true value of E_c is close to the upper bound of E_c (see main text section 2.1.1 and supplementary section S6). Therefore, $E_c + \Delta E \neq$ mDMA E' at low frequencies indicates that this assumption does not apply to the given sample, resulting in an incorrect estimate of E_c. Furthermore, since E_c is used to solve for the remaining material constants (equation 21 and 22, section 2.2), parameter estimates from the analysis procedure should not be trusted without additional validation.

S9.2 Cross-Validation using nDMA

If nDMA measurements are used as a control for cross-validation, and the same cantilever is used for bimodal and nDMA measurements, there will be no overlap between nDMA and bimodal AFM frequencies like there is with mDMA. As detailed in supplementary section S3.1, nDMA can only be performed at frequencies that do not correspond to cantilever resonances[13,14]. Therefore, bimodal AFM, which is performed at cantilever resonance frequencies, will not overlap with nDMA frequencies. However, bimodal measurements can be extrapolated from nDMA. For example, E_2' and $\tan\delta_1$ should not jump several orders of magnitude compared to E' or $\tan\delta$ at the closest nDMA frequency. Additionally, nDMA E' (calculated using the Hertz model as described in supplementary section S3) at low frequencies can be used to validate analysis procedure E_c in the same manner as mDMA. Also, in a similar manner to mDMA, the shape of reconstruction $E'(f)$, $E''(f)$, and $\tan\delta(f)$ curves should match nDMA curves if the SLS, MW, or KV models apply. However, if the GMM applies, nDMA and reconstruction curve shapes are unlikely to match (as in figure 5 and supplementary figure S2) because GMM curves are reconstructed using SLS equations (see main text section 2.3). Alternatively, a different cantilever from that used to perform bimodal imaging can be used to obtain nDMA measurements that overlap with bimodal AFM frequencies, thereby allowing cross-validation via nDMA measurements to be performed in the same manner as mDMA measurements.

Additionally, nDMA can synergize with mDMA and bimodal measurements to provide more information about a sample. For example, comparing nDMA and mDMA measurements can help determine the extent to which contact model selection and scaling behavior affect bimodal AFM measurements and analysis procedure outputs. Furthermore, combining nDMA with bimodal imaging eliminates the necessity of applying the analysis procedure beyond the model test (section 2.1) by providing more direct quantification of sample mechanics at low frequencies. This is a particular advantage because, as derived in section 2.1.1, the highest number of assumptions in the analysis procedure are made in order to estimate E_c, and thereby subsequent material parameters, from the model test fit to a GMM material. The necessity of making these assumptions can be avoided by employing nDMA in conjunction with bimodal imaging.

S9.3 Cross-Validation using Nanoindentation

Nanoindentation measurements can also be used to cross-validate analysis procedure E_c. In nanoindentation, the tip is pressed into

a sample, then withdrawn[21,27]. Sample indentation and the force experienced by the cantilever are tracked throughout[21,27]. Fitting the resulting force indentation curve with a contact model allows quantification of a sample's elastic modulus[21,27], or for more advanced contact models, the viscoelastic properties of SLS, KV, or MW materials[34]. Typically, nanoindentation is performed at slow indentation speeds relative to bimodal AFM, and the resulting elastic modulus therefore describes elastic behavior at low frequencies[13]. Since $E' \rightarrow E_c$ as $f \rightarrow 0$ for the GMM, SLS, and KV models (supplementary table S1), the elastic modulus from indentation experiments should be on a similar order of magnitude to E_c from the analysis procedure. If more advanced contact models that account for viscoelasticity are applied to indentation curves[34], and the model test indicates that the sample obeys the SLS, MW, or KV models, then E_c, E_r, and η calculated from indentation experiments can be compared against analysis procedure outputs. If the sample obeys the GMM, E_r and η may not match those of indentation experiments, since the analysis procedure is forced to approximate a GMM as an SLS and the resulting parameter estimates therefore only describe a subset of the sample's response (see paper section 2.1.1, figure 5 and supplementary figure S2). Additionally, the shape of the force indentation curve indicates whether the contact is adhesive, and therefore whether the Hertz model is an accurate description of the tip/sample interaction during bimodal AFM[34].

S9.4 Cross-Validation using Relaxation and Creep Measurements

Another means of cross-validating analysis algorithm outputs is relaxation or creep experiments. Both creep and relaxation can be measured at the macroscale or nanoscale[21,27,34]. Relaxation experiments maintain a constant strain (indentation) and observe how stress (force) changes through time, while creep experiments maintain constant stress (force) and observe how strain (indentation) changes through time[21,27,34]. For the GMM, SLS, KV, and MW models, stress through time during a relaxation experiment is dictated by an exponential with time constant τ_r[21,27,34]. Similarly, creep is dictated by an exponential with time constant τ_c[21,27,34]. Therefore, fitting exponentials to creep and relaxation measurements provides an alternate means of quantifying τ_r and τ_c that can be used to cross-validate analysis procedure outputs. If the sample is a KV material, creep experiment τ_c should match analysis procedure τ_c, and the sample will not relax during a relaxation experiment. If the sample is a MW material, analysis procedure τ_r should have a similar value to relaxation experiment τ_r, and both analysis procedure and creep experiment τ_c should be infinite. If the sample obeys the SLS or GMM, relaxation experiment τ_r should match analysis procedure τ_r and creep experiment τ_c should match analysis procedure τ_c.

S9.5 Cross-Validation using Literature Measurements

If it is not possible to obtain mDMA, nDMA, indentation, creep, or relaxation measurements of a sample to validate against analysis procedure outputs, it is still possible to compare procedure outputs against literature measurements of similar samples via similar steps described for each type of cross-validation measurement. In this case, emphasis should be placed on determining whether analysis procedure outputs have a similar order of magnitude to literature values, since the exact values of the given sample are unknown. For example if E_c of similar samples in the literature is 400 MPa, then sample E_c calculated by the analysis procedure should also be a few hundred MPa.

S9.5.1 Notes for Difficult Samples

It is important to note that nDMA can only be performed on thick samples (details in supplementary section S3.1)[13,14]. Additionally, indentation, nanoscale creep, and nanoscale relaxation measurements are sometimes difficult to perform on thin samples. For example, many biological samples that consist of individual biomolecules can be difficult to indent, let alone dwell on the sample to measure creep or relaxation, because such samples are only a few nm thick and can be easily displaced by the tip unless sample processing, which could alter material properties, is employed to fix the molecule in place. Additionally, for thin samples, the underlying substrate can affect indentation results, and must be accounted for in the contact model[35]. Furthermore, mDMA cannot always easily be employed in the place of nanoscale measurements of single-molecule samples because ensemble properties are not always the same as the properties of individual polymers[33]. For example, a molecule may not have the same properties in isolation compared to when the molecule is incorporated in a polymeric matrix because the molecule experiences different interactions and configurations in each environment[2,33]. In such circumstances, where all cross-validation measurements are difficult to perform, the cross-validation experiment with the highest chance of success would be nanoindentation with detailed analysis of the force indentation curves and contact model[34] or comparison against literature values.

S10 Supplementary Figures and Tables

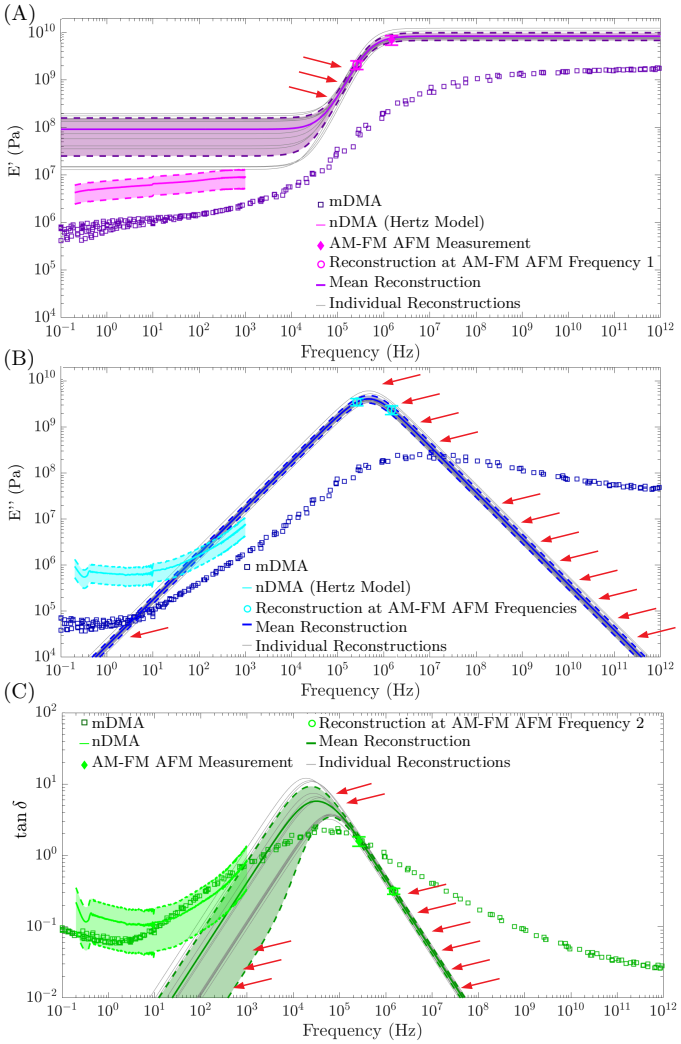

Fig. S2 Frequency dependent behavior of the SBR (AC160TSA). Storage moduli (E'), loss moduli (E''), and loss tangents ($\tan\delta$) over a range of frequencies are shown in (A), (B), and (C), respectively. Mean AM-FM AFM reconstructions are compared to control macroscale dynamic mechanical analysis (mDMA, squares) and nanoscale DMA (nDMA, lines) measurements. All data besides the reconstructions have been published previously[14], and are used here with permission. AM-FM AFM reconstructions from each of the 13 individual AM-FM AFM images are also shown in gray. Red arrows indicate regions where the reconstruction deviates from the controls by failing to account for all arms in the GMM. E' and E'' for nDMA were calculated using the Hertz contact model. AM-FM AFM and nDMA were performed using an AC160TSA cantilever. Error bars and shading represent the standard deviation.

Table S2 Model test metrics for each individual AM-FM AFM image of the sterine-butadiene rubber (SBR). In amplitude modulation-frequency modulation atomic force microscopy (AM-FM AFM), the AFM cantilever is vibrated at two eigenmodes. The loss tangent of a sample is measured via the lower eigenmode vibration ($\tan\delta_1$), and the storage modulus of the sample via the higher eigenmode vibration (E_2'). As derived in section 2.1 of the main article, a plot of $\tan\delta_1^{-1}$ vs. $(E_2'\tan\delta_1)^{-1}$ should be linear if the sample obeys the general Maxwell model (GMM), standard linear solid (SLS), Kelvin-Voigt (KV) or Maxwell (MW) model (equation 12). In other words, fitting a line to $\tan\delta_1^{-1}$ vs. $(E_2'\tan\delta_1)^{-1}$ should have high goodness of fit metrics, in this case R^2 value, if any of these four models can be used to describe the sample. If both the slope (m) and y-intercept (b) are greater than zero, the sample obeys the SLS or the GMM. If $m=0$ and $b>0$, the sample is a MW material. If $m>0$ and $b=0$, the sample is a KV material. Linear regression metrics detailing fit R^2, m, and b of the model test line (equation 12) to data from each individual AM-FM AFM image of the SBR are shown below. Measurements of the SBR were performed using AC240TSA and AC160TSA cantilevers. Numbers in parenthesis indicate the 95% confidence interval.

Cantilever	Image Number	Slope (95% Confidence Interval)	y-Intercept (95% Confidence Interval)	Fit R^2
AC240TSA	1	3.5642×10^8 (3.5639×10^8 - 3.5645×10^8)	0.2355 (0.2354 - 0.2357)	0.9966
	2	3.3664×10^8 (3.3658×10^8 - 3.3669×10^8)	0.2506 (0.2504 - 0.2507)	0.9886
	3	3.2344×10^8 (3.2342×10^8 - 3.2347×10^8)	0.2308 (0.2307 - 0.2309)	0.9979
	4	3.2675×10^8 (3.2672×10^8 - 3.2677×10^8)	0.2310 (0.2308 - 0.2311)	0.9972
	5	3.5771×10^8 (3.5706×10^8 - 3.5836×10^8)	0.2107 (0.2106 - 0.2108)	0.9448
	6	3.0099×10^8 (3.0052×10^8 - 3.0146×10^8)	0.2706 (0.2705 - 0.2707)	0.9598
	7	2.9664×10^8 (2.9621×10^8 - 2.9707×10^8)	0.2520 (0.2520 - 0.2521)	0.9649
	8	2.9058×10^8 (2.9017×10^8 - 2.9099×10^8)	0.2594 (0.2593 - 0.2595)	0.9667
	9	2.7743×10^8 (2.7743×10^8 - 2.7744×10^8)	0.2678 (0.2677 - 0.2680)	0.9997
	10	2.7808×10^8 (2.7806×10^8 - 2.7810×10^8)	0.2605 (0.2604 - 0.2607)	0.9976
	11	2.7392×10^8 (2.7390×10^8 - 2.7395×10^8)	0.2665 (0.2664 - 0.2667)	0.9973
	12	3.2635×10^8 (3.2634×10^8 - 3.2637×10^8)	0.2191 (0.2189 - 0.2192)	0.9985
	13	2.6619×10^8 (2.6614×10^8 - 2.6623×10^8)	0.2788 (0.2787 - 0.2789)	0.9957
	14	2.4033×10^8 (2.4005×10^8 - 2.4060×10^8)	0.2375 (0.2375 - 0.2376)	0.9684
	15	1.0957×10^8 (1.0956×10^8 - 1.0957×10^8)	0.2239 (0.2236 - 0.2242)	0.9999
	16	0.3467×10^8 (0.3467×10^8 - 0.3468×10^8)	0.3873 (0.3869 - 0.3876)	0.9996
	17	0.4585×10^8 (0.4585×10^8 - 0.4585×10^8)	0.4999 (0.4991 - 0.5006)	0.9997
	18	0.6107×10^8 (0.6107×10^8 - 0.6107×10^8)	0.4464 (0.4457 - 0.4470)	0.9999
	19	0.6760×10^8 (0.6754×10^8 - 0.6766×10^8)	0.3608 (0.3606 - 0.3611)	0.9768
	20	0.5735×10^8 (0.5732×10^8 - 0.5739×10^8)	0.3590 (0.3587 - 0.3593)	0.9891
	21	0.4519×10^8 (0.4519×10^8 - 0.4519×10^8)	0.5334 (0.5330 - 0.5338)	1.0000
	22	0.6144×10^8 (0.6144×10^8 - 0.6144×10^8)	0.3258 (0.3255 - 0.3261)	1.0000
	23	0.6744×10^8 (0.6737×10^8 - 0.6751×10^8)	0.3284 (0.3282 - 0.3285)	0.9807
	24	0.6417×10^8 (0.6411×10^8 - 0.6423×10^8)	0.3150 (0.3148 - 0.3151)	0.9843
	25	0.5195×10^8 (0.5195×10^8 - 0.5196×10^8)	0.6751 (0.6744 - 0.6757)	1.0000
AC160 TSA	1	7.7580×10^9 (7.7534×10^9 - 7.7625×10^9)	0.1634 (0.1631 - 0.1637)	0.9628
	2	6.5660×10^9 (6.5629×10^9 - 6.5691×10^9)	0.1481 (0.1479 - 0.1482)	0.9823
	3	5.4292×10^9 (5.4258×10^9 - 5.4326×10^9)	0.1270 (0.1268 - 0.1272)	0.9822
	4	3.7682×10^9 (3.7568×10^9 - 3.7796×10^9)	0.1857 (0.1855 - 0.1859)	0.8671
	5	5.1142×10^9 (5.1114×10^9 - 5.1169×10^9)	0.1224 (0.1223 - 0.1226)	0.9917
	6	4.9598×10^9 (4.9576×10^9 - 4.9619×10^9)	0.1507 (0.1505 - 0.1509)	0.9952
	7	4.8194×10^9 (4.8146×10^9 - 4.8243×10^9)	0.1681 (0.1678 - 0.1684)	0.9612
	8	5.1104×10^9 (5.1047×10^9 - 5.1161×10^9)	0.1558 (0.1555 - 0.1561)	0.9484
	9	4.1941×10^9 (4.1837×10^9 - 4.2045×10^9)	0.2412 (0.2408 - 0.2417)	0.8553
	10	5.3375×10^9 (5.3302×10^9 - 5.3448×10^9)	0.1710 (0.1706 - 0.1713)	0.9158
	11	5.3906×10^9 (5.3840×10^9 - 5.3973×10^9)	0.1781 (0.1778 - 0.1783)	0.9407
	12	4.8897×10^9 (4.8831×10^9 - 4.8962×10^9)	0.2133 (0.2130 - 0.2135)	0.9416
	13	4.7165×10^9 (4.7109×10^9 - 4.7220×10^9)	0.2176 (0.2173 - 0.2179)	0.9555

Notes and references

1 J. D. Ferry, *Viscoelastic properties of polymers*, Wiley, 3rd edn, 1980.

2 M. Doi, *Soft matter physics*, Oxford University Press, First edition edn, 2013.

3 V. L. Popov, M. Heß and E. Willert, *Handbook of Contact Mechanics: Exact Solutions of Axisymmetric Contact Problems*, Springer Berlin Heidelberg, 2019.

4 C. Adam, *Physical Regulation of Cell Behaviors: Multifrequency AFM Measurement of Mechanoelectric, Mechanochemical, and Hydration Shell Effects on ECM and Cell Substrate Viscoelasticity*, 2021.

5 B. Xu, H. Li and Y. Zhang, *Biomatter*, 2013, **3**, e24651.

6 R. Y. Dhume and V. H. Barocas, *Acta Biomaterialia*, 2019, **87**, 245–255.

7 J. Honerkamp and J. Weese, *Macromolecules*, 1989, **22**, 4372–4377.

8 N. Orbey and J. M. Dealy, *Journal of Rheology*, 1991, **35**, 1035–1049.

9 S. L. Hansen, P. M. Ray, A. O. Karlsson, B. Jørgensen, B. Borkhardt, B. L. Petersen and P. Ulvskov, *Plant Physiology*, 2011, **155**, 246–258.

10 D. Gutierrez-Lemini, *Engineering Viscoelasticity*, Springer, 2014.

11 R. S. Lakes, *Review of Scientific Instruments*, 2004, **75**, 797–810.

12 K. Menard, *Dynamic Mechanical Analysis: A Practical Introduction*, CRC Press, 2nd edn, 2008.

13 A. R. Piacenti, *Atomic Force Microscope-Based Methods for the Nano-Mechanical Characterisation of Hydrogels and other Viscoelastic Polymeric Materials for Biomedical Applications*, 2021.

14 A. R. Piacenti, C. Adam, N. Hawkins, R. Wagner, J. Seifert, Y. Taniguchi, R. Proksch and S. Contera, *Macromolecules*, 2024, **57**, 1118–1127.

15 T. Paavle, *Estonian Journal of Engineering*, 2011, **17**, 169–179.

16 P. C. Nalam, N. N. Gosvami, M. A. Caporizzo, R. J. Composto and R. W. Carpick, *Soft Matter*, 2015, **11**, 8165–8178.

17 T. Igarashi, S. Fujinami, T. Nishi, N. Asao and K. Nakajima, *Macromolecules*, 2013, **46**, 1916–1922.

18 H. K. Nguyen, M. Ito, S. Fujinami and K. Nakajima, *Macromolecules*, 2014, **47**, 7971–7977.

19 M. Arai, E. Ueda, X. Liang, M. Ito, S. Kang and K. Nakajima, *Japanese Journal of Applied Physics*, 2018, **57**, 08NB08.

20 E. Ueda, X. Liang, M. Ito and K. Nakajima, *Macromolecules*, 2019, **52**, 311–319.

21 H.-J. Butt, B. Cappella and M. Kappl, *Surface Science Reports*, 2005, **59**, 1–152.

22 G. Haugstad, *Atomic force microscopy: understanding basic modes and advanced applications*, John Wiley & Sons, 2012.

23 R. García, *Surface Science Reports*, 2002, **47**, 197–301.

24 R. Castro García, *Amplitude modulation atomic force microscopy*, 2011.

25 M. Kocun, A. Labuda, W. Meinhold, I. Revenko and R. Proksch, *ACS Nano*, 2017, **11**, 10097–10105.

26 A. Labuda, M. Kocuń, W. Meinhold, D. Walters and R. Proksch, *Beilstein Journal of Nanotechnology*, 2016, **7**, 970–982.

27 *Applications Guide Version 16 Revision*, Oxford Instruments Asylum Research Manual.

28 S. D. Solares and G. Chawla, *Measurement Science and Technology*, 2010, **21**, 125502.

29 S. Benaglia, V. G. Gisbert, A. P. Perrino, C. A. Amo and R. Garcia, *Nature Protocols*, 2018, **13**, 2890–2907.

30 R. Proksch and D. G. Yablon, *Applied Physics Letters*, 2012, **100**, 073106.

31 R. Proksch, M. Kocun, D. Hurley, M. Viani, A. Labuda, W. Meinhold and J. Bemis, *Journal of Applied Physics*, 2016, **119**, 134901.

32 E. T. Herruzo and R. Garcia, *Beilstein Journal of Nanotechnology*, 2012, **3**, 198–206.

33 R. Akhtar, M. J. Sherratt, J. K. Cruickshank and B. Derby, *Materials Today*, **14**, 96–105.

34 Y. M. Efremov, T. Okajima and A. Raman, *Soft Matter*, 2020, **16**, 64–81.

35 N. Gavara and R. S. Chadwick, *Nature Nanotechnology*, **7**, 733–736.